ACS APPLIED BIO MATERIALS

www.acsabm.org Article

M1 Macrophage-Derived Exosome-Mimetic Nanovesicles with an Enhanced Cancer Targeting Ability

Seungki Baek,[‖] Miyeon Jeon,[‖] Han Na Jung,[‖] Wooseung Lee, Jee-Eun Hwang, Jeong Seob Lee, Yeonjeong Choi, and Hyung-Jun Im*

Cite This: *ACS Appl. Bio Mater.* 2022, 5, 2862−2869 Read Online

ACCESS | Metrics & More | Article Recommendations | Supporting Information

ABSTRACT: Extracellular vesicles (EVs) have been found to be effective therapeutic drug delivery vehicles in a wide range of human diseases, including cancer and neurodegenerative diseases. Proinflammatory (M1) macrophages can modulate the suppressive immune environment of tumor tissues to be more inflammatory and have been considered as candidates for cancer immunotherapy. Furthermore, macrophage-derived exosome-mimetic nanovesicles (MNVs) could effectively induce antitumor response and enhance the efficacy of immune checkpoint inhibitors in a recent paper. However, multiple studies indicate that EVs were rapidly cleared by the reticuloendothelial system, and therefore, their tumor targeting efficiencies were limited. Herein, we developed a simple surface modification method of MNVs using polyethylene glycol (PEG) to enhance the in vivo tumor targeting efficiency. PEG-MNVs had 7-fold higher blood circulation than bare MNVs in the animal tumor model. Also, MNVs had a 25-fold higher protein amount than exosomes. Overall, the nanovesicle preparation strategies presented in this study may expedite the clinical translation of EV-based therapeutics in various diseases.

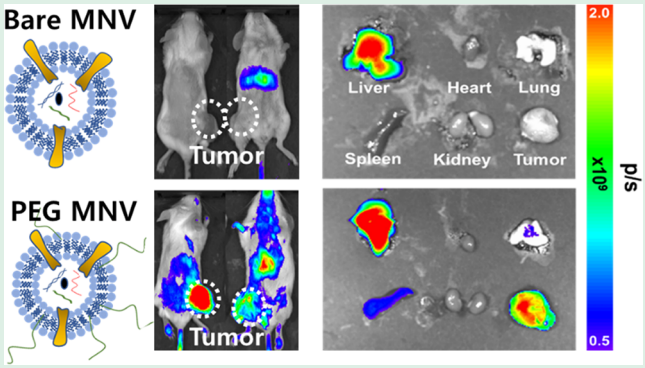

KEYWORDS: *exosome, extracellular vesicle, PEGylation, cancer, immunotherapy*

Downloaded via SEOUL NATL UNIV on July 19, 2022 at 02:52:11 (UTC).
See https://pubs.acs.org/sharingguidelines for options on how to legitimately share published articles.

■ INTRODUCTION

Extracellular vesicles (EVs) are a heterogeneous group of nanovesicles surrounded by a lipid bilayer and contain various cellular molecules including nucleic acids, peptides, proteins, and metabolites.[1,2] Various types of EVs have been identified including exosomes, ectosomes, microvesicles, and apoptotic bodies. In various forms of life, EVs are biological mediators that are used in cell to cell communication.[3] In recent years, EVs are widely utilized in bioinformatics and liquid biopsy since the biomolecules can be well-preserved in EVs.[4] Also, EVs are a promising drug delivery platform due to their biocompatibility and intrinsic tissue homing effect. Specific cell-derived exosomes demonstrated therapeutic potential on various human diseases.[5,6]

EVs have shown anticancer effects in various preclinical settings, and several clinical trials are underway.[7] Chemotherapeutic agent-loaded EVs have shown promising anticancer effects in various types of cancer models.[8,9] Also, mesenchymal stem cell-derived EVs loaded with an anti-KRAS siRNA showed effective tumor growth suppression in a mouse model of pancreatic cancer and are currently recruiting patients for phase 1 clinical trials (NCT03608631).[10] EVs can be used as cancer immunotherapy agents.[11] In particular, proinflammatory M1 macrophage-derived EVs demonstrated antitumor effects by immune modulation of the tumor microenvironment.[12−15] Choo et al. reported that M1 macrophage-derived nanovesicles can enhance the anticancer effect of immune checkpoint inhibitors by modulating anti-inflammatory tumor-associated macrophages.[12]

One of the main challenges for clinical translation of EV therapeutics including M1 macrophage-derived EVs is that EVs are rapidly eliminated by the reticuloendothelial system (RES) after systemic administration.[7] Hwang et al. reported that ^{99m}Tc-labeled EVs are quickly eliminated from the circulation and accumulated to the liver.[16] Herein, we developed a simple and effective PEGylation method for enhancing tumor targeting efficiency of M1 macrophage-derived exosome-mimetic nanovesicles (MNVs). First, we obtained MNVs by the cell extrusion method, which had a 25-fold higher protein amount than exosomes using the same number of cells. Furthermore, a simple method for PEGylation of MNVs

Received: March 17, 2022
Accepted: April 28, 2022
Published: May 13, 2022

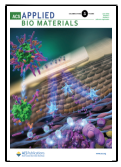

© 2022 American Chemical Society

https://doi.org/10.1021/acsabm.2c00246
ACS Appl. Bio Mater. 2022, 5, 2862−2869

improved the blood circulation and the cancer targeting ability. With consistent MNV size distribution after PEGylation (PEG-MNVs), the surface charge was neutralized. Remarkably, PEG-MNVs showed 7-fold higher tumor accumulation than bare MNVs. This preparation method can be a promising strategy to facilitate the clinical translation of various EV therapeutics.

■ RESULTS AND DISCUSSION

Characterization of M1 Macrophages for MNV Preparation. The M1 macrophage was induced using Raw 264.7 cells by LPS and IFN-γ. An MNV was prepared by an extrusion method using the M1 macrophage, which showed a cancer immune modulating effect in a previous study.[12]

Characterization of the M1 macrophage was performed by reverse transcription polymerase chain reaction (RT-PCR) and flow cytometry. Relative protein expression of proinflammatory markers, TNFα and iNOS, was observed by flow cytometry. As shown in Figure 1a,b, the M1 macrophage showed larger shifts of TNFα and iNOS expression than the uninduced M0 macrophage. Correspondingly, RT-PCR was conducted to evaluate the representative M1 marker CD86 and iNOS mRNA quantity. Both factors were normalized with GAPDH, and whole primer sequences are introduced in Figure S1. Figure 1c indicated a much higher M1 mRNA quantity of CD86 and iNOS than that of M0 mRNA. Successful M1 macrophage induction was confirmed by increased expression of CD86, iNOS, and TNFα in M1 macrophages.

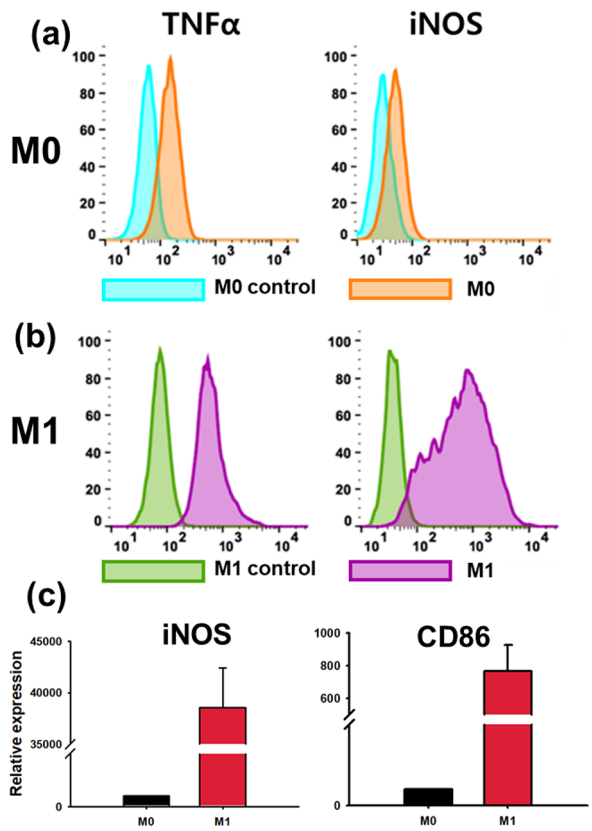

Figure 1. Comparison of the relative gene expression between M0 macrophages and M1 macrophages. M0 and M1 were analyzed with proinflammatory markers. TNFα and iNOS signals were observed with flow cytometry. Each cell phenotype has a nonantibody-treated group as a control (a,b). RT-PCR analyzed data with relative CD86 and iNOS mRNA expression in M0 and M1 macrophages (c). Data were indicated as the mean ± standard deviation. Amounts of genes of interests were normalized to GAPDH.

Biochemical and Physiological Characterization of Exosomes and MNVs. To measure the size and compare the morphology, MNV images were acquired with an energy-filtering transmission electron microscope (EF-TEM) (Figure 2a). Both exosomes and MNVs showed similar size distribution (~200 nm) and spherical morphologies through the images. Subsequently, the protein amounts of MNVs and exosomes from the same number of cells (5×10^7 cells) were measured with a BCA assay. We found that MNVs have a 25-fold higher protein amount than exosomes (Figure 2b). These results are similar to those of previous studies, and therefore, we emphasize that the extrusion method for producing exosome-mimetic nanovesicles can be considered as a good candidate for clinical translation of EVs. Each sample was isolated and quantified to determine the similarity of protein components between cytosolic proteins, membrane proteins, and MNVs. Western blotting was conducted with the same protein amount of cytosolic proteins, membrane proteins, and MNVs from M1 macrophages. MNVs showed a similar expression level of Alix, an exosome marker, with membrane proteins (Figure 2c and Figure S2).

Size and Stability of Bare MNVs and PEG-MNVs. Using PEG_{2k} in liposome production is the most widely used PEG length, and Pozzi et al. reported that PEG_{2k} has a higher cellular uptake than PEG_{1k} and PEG_{5k}.[17,18] In addition, our group has performed several studies preparing liposomes using PEG_{2k} that were reproducible and stable over time.[19,20] Therefore, MNVs were PEGylated using DSPE-PEG_{2k} and purified using a PD-10 desalting column. EF-TEM examination demonstrated that both MNVs were similar in size and shape. Both bare MNVs and PEG-MNVs had round vesicle shapes (Figure 3a,b). Hydrodynamic sizes were correlated with EF-TEM data. The size distributions of bare MNVs and PEG-MNVs were 177.0 ± 70.56 and 184.9 ± 50.30 nm, respectively (Figure 3c,d). Additionally, the polydispersity index (PDI) indicated that PEG-MNVs were much monodisperse than bare MNVs (Figure 3e), possibly due to the stabilizing effect of PEG. The result is consistent with that of a previous paper demonstrating a smaller PDI of PEGylated liposomes than that of bare liposomes.[21]

To confirm the surface charge of bare MNVs and PEG-MNVs, the zeta potential was measured with DLS. In Figure 3f, PEG-MNVs showed a more neutral surface charge than bare MNVs (−5.91 ± 4.02 vs −43.4 ± 7.04 mV, respectively). Also, neutralization can be an indication of successful PEGylation because it is reported that PEGylation can reduce the surface charge of liposomes.[22] A neutral surface charge is a favorable feature for a longer in vivo circulation in the blood vessel because negatively charged nanoparticles can avoid the opsonization of protein in blood. The function of PEGylation is known as the stealth effect.[23]

As described in a previous paper,[19] the stability test of MNVs was conducted in PBS for 7 days. By measuring the size and PDI at each time point, they showed the stability of MNVs for 7 days without remarkable size changes (Figure 3g). This could predict well in vivo stability after intravenous injection of MNVs.

Next, we synthesized DiR-labeled PEG-MNVs. Also, we performed the stability test of PEG-MNVs after DiR fluorescence labeling, which showed a stable size distribution

https://doi.org/10.1021/acsabm.2c00246
ACS Appl. Bio Mater. 2022, 5, 2862−2869

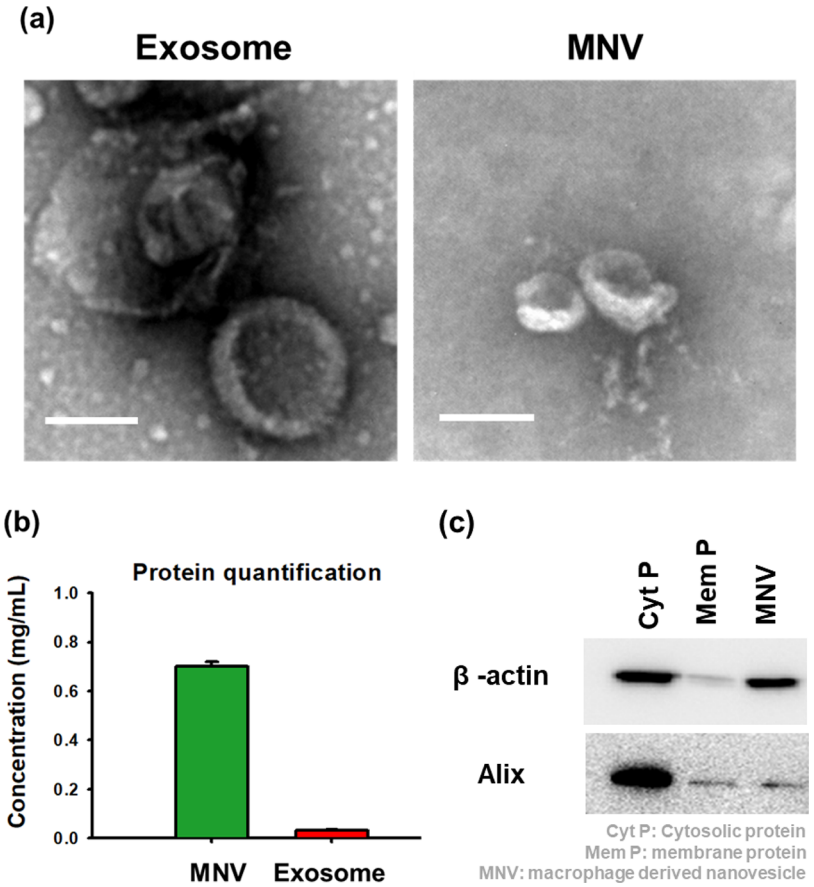

Figure 2. Physical and biochemical characteristics of exosomes and MNVs. EF-TEM images (a), white scale bar: 100 nm. Protein quantification of MNVs and exosomes (b). Western blotting of β-actin and Alix (c).

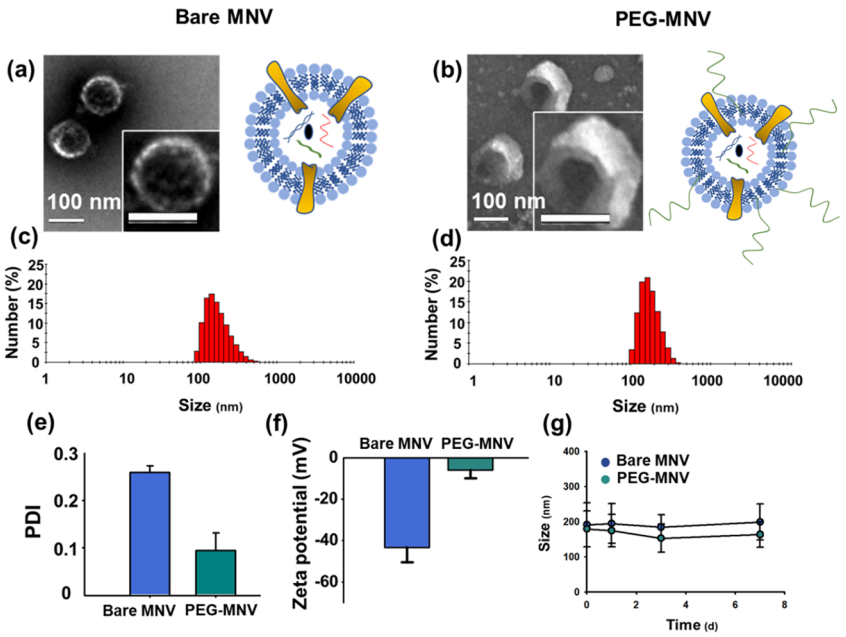

Figure 3. Physical characterization of bare MNVs and PEG-MNVs. EF-TEM images of bare MNVs (a) and PEG-MNVs (b) (white scale bar: 100 nm). Hydrodynamic sizes of bare MNVs (c) and PEG-MNVs (d). Polydispersity index (e) and zeta potential (f) of both MNVs. (g) Stability testing of bare MNVs and PEG-MNVs in PBS for 7 days (n = 4, mean ± standard deviation).

and PDI for 7 days in PBS (Figure S3). Since the method of preparing DiR-labeled PEG-MNVs includes the process of adding DiR and DSPE-PEG$_{2k}$ to the MNV solution, self-assembled micelles composed of DiR and DSPE-PEG$_{2k}$ may be formed as byproducts. Thus, we performed a similar experimental process using DiR, DSPE-PEG$_{2k}$, and a solution

https://doi.org/10.1021/acsabm.2c00246
ACS Appl. Bio Mater. 2022, 5, 2862−2869

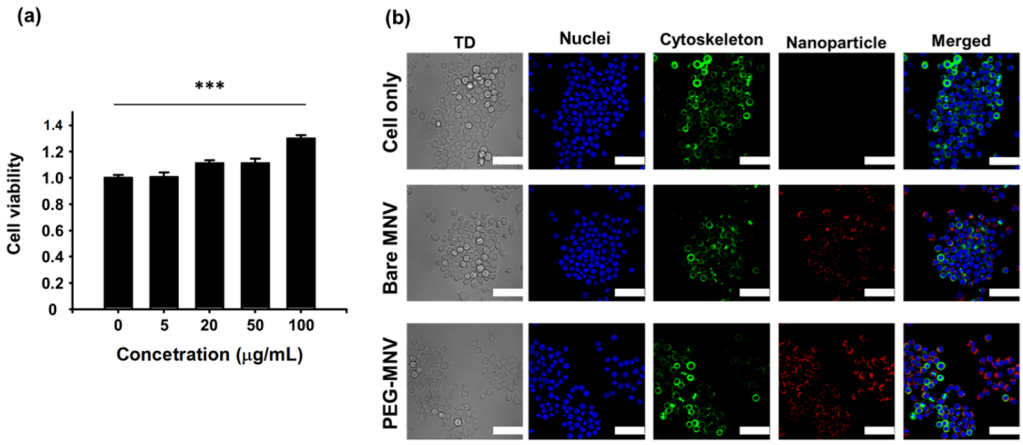

Figure 4. Cytotoxicity and cellular uptake (n = 3). Cytotoxicity was performed using an MTT assay with the M2 macrophage. Five different concentrations of PEG-MNVs were treated to cells (a). Confocal images of DiR-labeled bare MNVs and PEG-MNVs internalized in the M2 macrophage (b) (blue: Hoechst 33342 for the nucleus; green: ViaFluor 488 for microtubule staining; red: nanoparticle intercalated DiR); ***P < 0.005, Student's t-test was conducted for statistics.

without MNVs to test if DiR and DSPE-PEG$_{2k}$ can form micelles. However, when a mixture of DiR and DSPE-PEG$_{2k}$ was loaded into the PD-10 column, the fluorescence component was captured by the column, indicating that the DiR-labeled nanostructures were not formed by the process. On the other hand, the fluorescence signal can be easily filtered out when DiR-labeled PEG-MNVs were loaded into the column. Also, no nanostructures could be found in the DiR + DSPE-PEG$_{2k}$ mixture by EF-TEM images (Figure S4), confirming that no byproducts were formed that could confound the interpretation of subsequent imaging experiments.

Influence of PEG-MNVs on M2 Macrophages. In vitro cytotoxicity testing of PEG-MNVs was performed to determine the toxicity on a cellular level. All experiments were conducted with IL-4-activated M2 macrophage cells, which are known to be similar to tumor-associated macrophages. Since we hypothesized the potential of therapeutic effects of immune modulation by M1 macrophage-derived MNVs, a cytotoxicity test was performed with M2 macrophages from the highest concentration of 100 μg/mL to 0 μg/mL PEG-MNVs in PBS. As shown in Figure 4a,b, there was no cytotoxicity of PEG-MNVs to M2 macrophages. Intriguingly, at the highest concentration (100 μg/mL), the number of M2 macrophages was significantly increased. As many previous studies reported, M1 macrophages in the reprogramming proliferated more than M2 macrophages.[24] Thus, we speculated that the M2 macrophages were reprogrammed to M1 macrophages by PEG-MNVs.

Bare MNVs and PEG-MNVs were fluorescently labeled, as shown in Figure 5, to assess the cellular uptake of the particles. Cellular uptake tests were conducted in induced M2 macrophages after staining by Hoechst 33342 and ViaFluor 488 for nuclei and the cytoskeleton, respectively. The cellular uptake efficiency of bare MNVs and PEG-MNVs was similar, indicating that surface modification of MNVs did not alter the ability of MNVs to enter the M2 macrophages.

In Vivo Passive Tumor Targeting Effect. Finally, we assessed the tumor targeting ability of PEG-MNVs using in vivo and ex vivo fluorescence imaging. For the in vivo imaging experiments, DiR-labeled bare MNVs and PEG-MNVs were injected intravenously to compare the tumor targeting

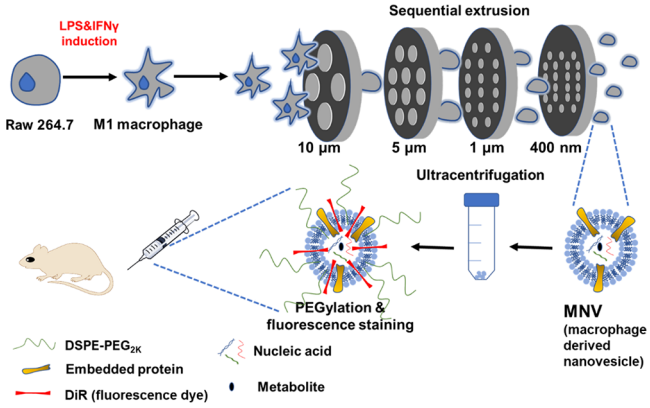

Figure 5. Schematic illustration from the MNV preparation to the animal experiment of the DiR-labeled PEG-MNV. Following the cell activation, sequential extrusion, ultracentrifugation, and surface modification, MNVs were applied to the mice.

efficiency in CT26 tumor-bearing mice. We found that PEG-MNVs exhibited significantly higher tumor uptake than bare MNVs for both in vivo and ex vivo imaging (Figure 6a,b). Tumor uptake was examined and quantitatively compared between the bare MNV- and PEG-MNV-injected groups through tumor to liver ratio calculation. The tumor to liver ratio of PEG-MNVs was 7-fold higher than that of bare MNVs (Figure 6c). Correspondingly, Figure S5 shows a higher accumulation of PEG-MNVs than bare MNVs in the sectioned tumor.

All animal studies were performed with six-weeks-aged BALB/c mice (n = 5). As reported in another exosome study,[25] an injection dose of MNVs should not be over 400 μg to avoid severe side effects or unwanted death by blocking the lung microcapillaries of mice. In this animal work, we explored the in vivo toxicity of PEG-MNVs with histological analysis and blood tests. Normal mice were injected with 20 μg of MNVs to evaluate tissue damage through histological analysis. The organ histology of PEG-MNV-injected mice was similar to normal saline-injected mice (Figure S6), and there were no pathological abnormalities in the H&E results. Furthermore, the toxicity of the liver and kidney was also assessed by measuring the alanine transaminase (ALT), aspartate trans-

https://doi.org/10.1021/acsabm.2c00246
ACS Appl. Bio Mater. 2022, 5, 2862−2869

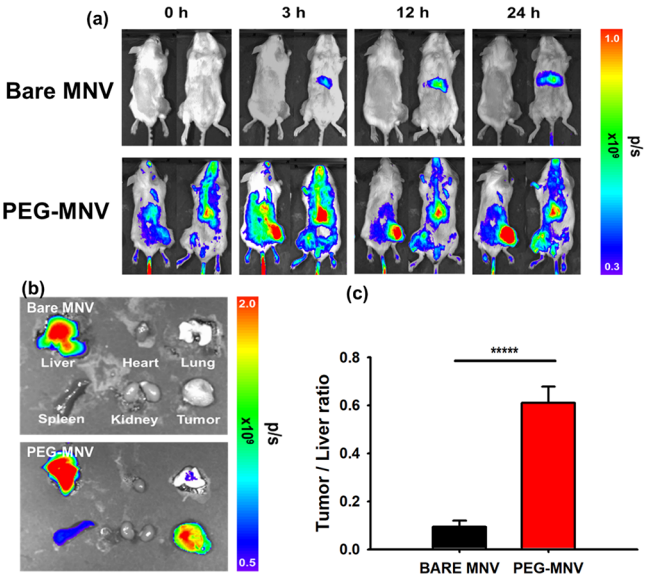

Figure 6. In vivo and ex vivo imaging and analysis. CT26 tumor model (n = 5) at 0, 3, 12, and 24 h after i.v. injection of bare MNVs and PEG-MNVs. In vivo (a) and ex vivo imaging (b). Quantitative analysis with the tumor to liver ratio (c). *****P < 0.00005. Student's t-test was conducted for statistics.

aminase (AST), blood urea nitrogen (BUN), and creatinine (Cr) 14 days after injection of PEG-MNVs or saline. The values of the toxicity tests were within the normal range. Values of the PEG-MNV-injected group have no significant difference from the values of the normal saline-injected group (Figure S7).

Various engineering methods are actively applied to EVs to enhance targeting efficiency and therapeutic effects.[26] There have been studies to enhance the circulation time and targeting efficiency of EVs by adding PEG or self-peptides.[7] Shi et al. demonstrated that PEGylated EVs had an increased tumor targeting ability using positron emission tomography (PET). In the study, PEG with amine-reactive moieties (NHS) was covalently conjugated to membrane proteins in EVs. In the PET imaging, tumor uptake and liver uptake were 2.7 ± 0.3 and 13.8 ± 0.9% ID/g, respectively, at 24 h after the injection.[27]

On the contrary to the previous study, we utilized DSPE-PEG_{2k} to integrate it into the lipid membrane of EVs. Membrane proteins would not be altered in our method as our method does not require covalent bonding. Moreover, although there is a difference in the imaging modalities, the quantified tumor to liver ratio was higher in our study than that of the previous study (this study = 0.6, Shi et al. = 0.2). Kamerkar et al. labeled EVs with a self-peptide, CD47, and the CD47-labeled EVs showed delayed clearance in the circulation. However, the tumor targeting ability of the engineered EVs has not been provided in the previous study.[10] Koojimans et al. reported a method for decorating EVs with PEG using PEG-micelles. They showed enhanced circulation time of the EVs after PEG decoration. However, there was no prominent uptake in the tumor in the IVIS imaging.[28] Also, Emam et al. used PEG-micelles for PEGylation of EVs.[29] In the previous study, the tumor uptake was evident in IVIS imaging; however, the quantitative tumor targeting ability was not compared to bare EVs.[29] The methods and efficiencies of the PEGylation method of EVs in previous and present studies are summarized in Table 1. Taken together, we presented a simple PEGylation method for enhancing the tumor targeting efficiency of M1-derived EVs, and this method appears to be superior to previously reported methods in terms of tumor targeting efficiency.

CONCLUSIONS

In this study, we developed PEG-MNVs from M1 macrophages with an enhanced tumor targeting ability. Experimental results show that the PEG-MNV has a 7-fold higher tumor targeting efficiency than bare MNVs. Therefore, PEG-MNVs appear to be a promising tool as a cancer immune modulating agent with a superior tumor targeting ability in the field of nanoparticle delivery systems. Furthermore, the simple MNV PEGylation method presented in this study can be applied to various types of EV therapeutics. It can further expand the study by developing nanovesicles using different cell lines and various cargo-loaded drugs to determine the therapeutic effects.

EXPERIMENTAL SECTION

Materials and Reagents. 1,2-Distearoyl-*sn*-glycero-3-phosphoethanolamine-*N*-[methoxy(polyethylene glycol)-2000] (DSPE-PEG_{2k}) was purchased from Avanti (Alabama, USA). 1,1′-Dioctadecyl-3,3,3′,3′-tetramethylindotricarbocyanine iodide (DiR) and a Superscript IV VILO master mix (VILO) were obtained from Invitrogen (Carlsbad, USA). Methyl alcohol was purchased from Daejung (Busan, Korea). A PD-10 column was purchased from GE Healthcare (Buckinghamshire, UK). All cell experiments were conducted with culture medium; Dulbecco's modified Eagle medium (DMEM), 10% fetal bovine serum (FBS), and 1% penicillin−streptomycin (PS) were purchased from Hyclone (Utah, USA). For living cell staining, nuclei were fluorescence labeled with Hoechst 33342 (Invitrogen, Carlsbad, USA), and microtubules were stained with ViaFluor 488 (Biotium, California, USA). For macrophage activation, a lipopolysaccharide (LPS) and interferon gamma (IFN-γ) and interleukin-4 (IL-4) were obtained from Invitrogen (Carlsbad, USA) and Peprotech (New Jersey, USA). RNA extraction was conducted using a TRIzol reagent (Thermo Fisher, Massachusetts, USA). A SYBR Green PCR kit (SYBR, Qiagen, Valencia, CA) was obtained for PCR. The cell viability test was performed with MTT solution (Thermo Fisher, Massachusetts, USA).

Instruments. To measure the size distribution of exosomes and MNVs, dynamic light scattering (DLS, Malvern Instruments Ltd., Worcestershire, UK) and energy-filtering transmission electron

Table 1. Comparison of PEGylation Methods of EVs[a]

studies	PEGylation method	type of PEG	imaging	targeting ability (tumor/liver ratio)
Shi et al. (2019)[27]	amine conjugation	NHS-PEG_{5k}	PET	0.2
Emam et al. (2021)[29]	PEG micelle	DSPE-PEG_{2k}	fluorescence imaging	N.R.
Koojimans et al. (2016)[28]	PEG micelle	DSPE-PEG_{2k}	fluorescence imaging	N.R.
this study	direct PEG-lipid addition	DSPE-PEG_{2k}	fluorescence imaging	0.6

[a]DSPE: 1,2-distearoyl-*sn*-glycero-3-phosphoethanolamine; N.R.: not reported; PET: positron emission tomography.

https://doi.org/10.1021/acsabm.2c00246
ACS Appl. Bio Mater. 2022, 5, 2862−2869

microscopy (EF-TEM, Carl Zeiss, Oberkochen, Germany) were employed. Absorbance data were obtained from a microplate reader (BioTek, Vermont, USA). In vivo biodistribution was observed with an in vivo imaging system (IVIS, PerkinElmer, Massachusetts, USA). Flow cytometry was conducted with a Guava easyCyte 5 (Millipore, Massachusetts, USA). Cell fluorescence and ex vivo tissue fluorescence images were acquired with a Nikon A1R (Nikon Co., Tokyo, Japan) and a Stellaris 5 (Leica Microsystems, Wetzlar, Germany). Total RNA was quantified using a Nanodrop spectrometer (Thermo Fisher, Massachusetts, USA). For purification and pelleting down, an ultracentrifuge (SW 32 Ti swing-bucket rotor package; Beckman Coulter-Optima XPN-100, California, USA) was used.

Cell Culture. The monocyte cell line Raw 264.7, which is known as the M0 macrophage, and the CT26 murine colon carcinoma cell line were obtained from Korea Cell Line Bank. They were cultured in DMEM with 10% FBS and 1% PS. The cells were incubated at 37 °C under 5% CO_2. For type I proinflammatory macrophage (M1 macrophage) induction, 100 ng/mL LPS and 20 ng/mL IFN-γ were added to the culture medium.[30] For type II anti-inflammatory macrophage (M2 macrophage) induction, 20 ng/mL recombinant murine IL-4 was added into the growth medium.

Animals. Under the guidelines of the Institutional Animal Care and Use Committee, Seoul National University, six-weeks-aged female BALB/c mice (Orient Bio, Seongnam, Korea) were utilized for in vivo stability and nanoparticle biodistribution. For the mouse tumor model, 3×10^6 CT26 cells were subcutaneously injected into the right flank of BALB/c mice. IVIS imaging was conducted when the tumor reached a mean diameter of 6−10 mm. To assess the biocompatibility of MNVs, six-weeks-aged female healthy BALB/c mice were used.

mRNA Isolation and Analysis. One microgram of total RNA from M0, M1, and M2 macrophages was prepared for cDNA synthesis via VILO. Quantitative real-time PCR (qRT-PCR) was performed with SYBR. The PCR cycle was to first heat activate for 2 min at 95 °C immediately followed by 40 cycles with two-step cycling, denaturation for 5 s at 95 °C, annealing, and extension for 10 s at 60 °C. All data were analyzed with three samples per group using the comparative Ct method. To evaluate the expression of M1 macrophage factors in M0 and M1 macrophages, forward and reverse primers of CD86, iNOS, and GAPDH were used. The primer sequences are listed in Figure S1.

Cell Flow Cytometry. To determine the differentiation rate of M1 macrophages, flow cytometry was conducted with representative proinflammatory factors TNFα and iNOS. For M1 macrophage differentiation, LPS- and IFN-γ-treated 1×10^6 Raw 264.7 cells were harvested overnight at 37 °C under 5% CO_2. Afterward, the eFluor710-conjugated antimouse monoclonal antibody (Invitrogen, 46-7321-80, 1:100) and the Alexa Fluor 488 antimouse monoclonal antibody (Invitrogen, 53-5920-82, 1:200) were added in 500 μL cell solutions for 2 h and kept in an ice bath. Then, they were washed twice with 500 μL of FACS buffer. Flow cytometry data were obtained on a Guava easyCyte 5. The cells were initially identified and gated by side scattering and forward scattering for the analysis using FlowJo v10 (FlowJo, LLC). Each factor was compared with the M0 macrophage control group.

Preparation of Exosomes and Macrophage-Derived Nanovesicles (MNVs). MNVs were prepared with sequential extrusion of M1 macrophages. LPS- and IFN-γ-treated 5×10^7 M1 macrophages were incubated in 11 mL of PBS. Suspended cells were sequentially extruded 10 times through each of 10 μm, 5 μm, 1 μm, and 400 nm pore-sized polycarbonate membrane filters (Whatman, New Jersey, USA) using a miniextruder from Avanti (Alabama, USA). The pure MNVs were washed with 25 mL of PBS after the extrusion. Then, the pure MNVs were collected through an ultracentrifuge at 100,000*g* for 2 h. After discarding the supernatant, MNV pellets were resuspended and filtered with a 0.20 μm cellulose acetate filter (Advantec, Tokyo, Japan).

Surface Modification of MNVs. Forty microliters of 25 mg/mL DSPE-PEG_{2k} was prepared in chloroform. Then, chloroform was removed through evaporation in a vacuum chamber for 12 h. Following evaporation, 10 μL of methyl alcohol was added to the DSPE-PEG_{2k} lipid layer. The DSPE-PEG_{2k} in methanol solution and 0.2 μg of DiR were mixed with 100 μg of previously prepared MNVs in 400 μL of PBS solution. Reactions were conducted for an hour at 37 °C with constant shaking on an orbital shaker. Then, DiR-labeled MNVs were purified using a PD-10 desalting column in PBS.

Protein Isolation Analysis. A Mem-PER (Thermo Fisher, Massachusetts, USA) was used to obtain the membrane proteins and cytosolic proteins from 5×10^6 Raw 264.7 cells. Cells were briefly treated with solubilization buffer and permeabilization buffer to isolate the membrane proteins and cytosolic proteins. The amounts of the membrane proteins, cytosolic proteins, exosomes, and MNVs were analyzed by a Pierce BCA protein assay kit (Thermo Fisher, Massachusetts, USA). Absorbance data were acquired using a microplate reader.

Western blotting was performed to detect β-actin and Alix in membrane proteins, cytosolic proteins, exosomes, and MNVs derived from Raw 264.7. Briefly, each sample was loaded into 10% polyacrylamide gels and transferred on PVDF membranes (Millipore, MA, USA). Protein-transferred membranes were blocked with skimmed milk and then treated with an antimouse monoclonal antibody from Santa Cruz (SC-47778, 1:1000) and an antimouse monoclonal antibody from Cell Signaling Technology (no. 2171, 1:1000). A purchased antimouse HRP-conjugated secondary antibody (Invitrogen, no. 31430, 1:5000) was used with a SuperSignal West Pico PLUS chemiluminescent substrate (Thermo Fisher, Massachusetts, USA) for chemiluminescence reactions. Protein bands were analyzed using Chemidoc (BioRad, Hercules, CA).

Characterization of Exosomes, Bare MNVs, and PEGylated MNVs. The morphologies of exosomes, bare MNVs, and PEGylated MNVs were observed using an EF-TEM. Zeta potentials and hydrodynamic sizes of bare MNVs and PEGylated MNVs were measured by DLS. Each experiment was carried out in triplicate. The stability of bare MNVs and PEGylated MNVs was assessed for 7 days in distilled water and PBS.

Cellular Uptake. DiR-labeled bare MNVs and PEGylated MNVs were prepared to visualize the cellular uptake. Both bare MNVs and PEGylated MNVs were filtered with a PD-10 desalting column for purification. For differentiation to M2 macrophages of Raw 264.7 cells, which were applied with 20 ng/mL IL-4,[31] 1×10^5 cells were cultured in a confocal microscopy dish overnight at 37 °C under 5% CO_2. The DiR-labeled bare MNVs and PEGylated MNVs were applied and were incubated for 3 h. Then, cells were treated with Hoechst 33342 and ViaFluor 488 for nucleus and microtubule staining, respectively, for 1 h. After the incubation, cells were washed with DPBS twice. All observations were conducted with A1R confocal microscopy.

In Vitro Cytotoxicity. Raw 264.7 cells were equally plated into 96-well plates at 5×10^4 cells/well in DMEM medium supplemented with 10% FBS and 1% PS. Then, 20 ng/mL IL-4 was applied to cells and incubated overnight at 37 °C with 5% CO_2 for M2 polarization. Different concentrations of PEGylated MNVs in DPBS were added to cells, which were incubated overnight. After washing cells with DMEM to discard PEGylated MNVs from the culture medium, MTT solution was then added to the cells for 6 h. The MTT solution was removed, and DMSO (100 μL/well) was subsequently added to formazan. The absorbance data were acquired through a microplate reader at 540 nm.

In Vivo Fluorescence Imaging and Analysis. CT26-inoculated BALB/c mice were utilized for fluorescence imaging. As illustrated in Figure 5, DiR-labeled bare MNVs and PEGylated MNVs were prepared and intravenously injected at 20 μg of MNV/mice through the tail vein (n = 5). IVIS images were taken after 24 h of injection. The mice were ethically euthanized under anesthesia with isoflurane for ex vivo studies. The tumor, liver, spleen, heart, lungs, and kidney were collected. All ex vivo fluorescence images were acquired using IVIS. The conditions for imaging were as follows: excitation, 740 nm; emission, 790 nm; exposure, 15 s; binning factor, 4. The tumor to organ ratio was statistically analyzed with a two-sided Student's *t*-test.

H&E Staining and Blood Tests. To determine tissue damage, major organs were collected 14 days after the injection via the tail

https://doi.org/10.1021/acsabm.2c00246
ACS Appl. Bio Mater. 2022, 5, 2862−2869

vein. For the biocompatibility test, the liver, heart, spleen, kidney, and lungs were obtained from the MNV-injected mice. To observe histological abnormalities, all organs were paraffin sectioned and H&E stained. Organs from the control group and the test group were observed with a microscope. Furthermore, the toxicity of MNVs was also assessed by renal and hepatic blood toxicity tests. Blood samples were collected in an EDTA+ vacutainer, and the test was performed with blood urea nitrogen (BUN), alanine transaminase (ALT), aspartate transaminase (AST), and creatinine (Cr). To compare the control group, normal saline was injected to the BALB/c mice. All blood tests were conducted with five mice per group.

■ ASSOCIATED CONTENT

Supporting Information

The Supporting Information is available free of charge at https://pubs.acs.org/doi/10.1021/acsabm.2c00246.

Primer sequences for qRT-PCR; full images of Western blotting with the sample from the M1 macrophage; comparison between the DiR + phospholipid mixture and DiR-labeled PEGylated MNVs; stability testing of DiR-labeled PEGylated MNVs using DLS; ex vivo fluorescence imaging of PEGylated MNV-injected mice; blood testing for in vivo toxicity (PDF)

■ AUTHOR INFORMATION

Corresponding Author

Hyung-Jun Im − *Department of Applied Bioengineering, Graduate School of Convergence Science and Technology and Department of Molecular Medicine and Biopharmaceutical Sciences, Graduate School of Convergence Science and Technology, Seoul National University, Seoul 08826, Republic of Korea; Cancer Research Institute, Seoul National University, 03080 Seoul, Republic of Korea; Research Institute for Convergence Science, Seoul National University, Seoul 08826, Republic of Korea;* orcid.org/0000-0002-4368-6685; Email: iiihjjj@snu.ac.kr, iiihjjj@gmail.com

Authors

Seungki Baek − *Department of Applied Bioengineering, Graduate School of Convergence Science and Technology, Seoul National University, Seoul 08826, Republic of Korea*

Miyeon Jeon − *Department of Applied Bioengineering, Graduate School of Convergence Science and Technology, Seoul National University, Seoul 08826, Republic of Korea*

Han Na Jung − *Department of Applied Bioengineering, Graduate School of Convergence Science and Technology, Seoul National University, Seoul 08826, Republic of Korea*

Wooseung Lee − *Department of Applied Bioengineering, Graduate School of Convergence Science and Technology, Seoul National University, Seoul 08826, Republic of Korea*

Jee-Eun Hwang − *Department of Molecular Medicine and Biopharmaceutical Sciences, Graduate School of Convergence Science and Technology, Seoul National University, Seoul 08826, Republic of Korea*

Jeong Seob Lee − *Department of Applied Bioengineering, Graduate School of Convergence Science and Technology, Seoul National University, Seoul 08826, Republic of Korea*

Yeonjeong Choi − *Department of Applied Bioengineering, Graduate School of Convergence Science and Technology, Seoul National University, Seoul 08826, Republic of Korea*

Complete contact information is available at: https://pubs.acs.org/10.1021/acsabm.2c00246

Author Contributions

[‖]S.B., M.J., and H.N.J. contributed equally as co-first authors. H.-J.I. and S.B. designed this project. S.B. and W.L. designed the nanovesicle and surface modification method. All assessments with statistical analysis were performed by M.J. and W.L. Y.C. participated in RNA experiments. J.-E.H. and J.S.L. supported the in vivo experiment. All authors have contributed to the completion of the manuscript.

Notes

The authors declare the following competing financial interest(s): Hyung-Jun Im is the Chief Scientific Officer of Portrai. Hyung-Jun Im is a consultant of Cellbion. Otherwise, there is no competing financial interest.

■ ACKNOWLEDGMENTS

This study was supported by the National Research Foundation of Korea (NRF) (NRF-2019M2D2A1A01058210, NRF-2020R1C1C1009000, and 2021M2E8A1039564) and the Creative-Pioneering Researchers Program through Seoul National University (SNU).

■ REFERENCES

(1) Théry, C.; Zitvogel, L.; Amigorena, S. Exosomes: composition, biogenesis and function. *Nat. Rev. Immunol.* **2002**, *2*, 569−579.

(2) van Niel, G.; D'Angelo, G.; Raposo, G. Shedding light on the cell biology of extracellular vesicles. *Nat. Rev. Mol. Cell Biol.* **2018**, *19*, 213−228.

(3) Mathieu, M.; Martin-Jaular, L.; Lavieu, G.; Théry, C. Specificities of secretion and uptake of exosomes and other extracellular vesicles for cell-to-cell communication. *Nat. Cell Biol.* **2019**, *21*, 9−17.

(4) Zhou, B.; Xu, K.; Zheng, X.; Chen, T.; Wang, J.; Song, Y.; Shao, Y.; Zheng, S. Application of exosomes as liquid biopsy in clinical diagnosis. *Signal Transduction Targeted Ther.* **2020**, *5*, 144.

(5) Saeedi, S.; Israel, S.; Nagy, C.; Turecki, G. The emerging role of exosomes in mental disorders. *Transl. Psychiatry* **2019**, *9*, 122.

(6) Sarko, D. K.; McKinney, C. E. Exosomes: Origins and Therapeutic Potential for Neurodegenerative Disease. *Front. Neurosci.* **2017**, *11*, 82.

(7) Herrmann, I. K.; Wood, M. J. A.; Fuhrmann, G. Extracellular vesicles as a next-generation drug delivery platform. *Nat. Nanotechnol.* **2021**, *16*, 748−759.

(8) Xu, R.; Rai, A.; Chen, M.; Suwakulsiri, W.; Greening, D. W.; Simpson, R. J. Extracellular vesicles in cancer — implications for future improvements in cancer care. *Nat. Rev. Clin. Oncol.* **2018**, *15*, 617−638.

(9) Jang, S. C.; Kim, O. Y.; Yoon, C. M.; Choi, D.-S.; Roh, T.-Y.; Park, J.; Nilsson, J.; Lötvall, J.; Kim, Y.-K.; Gho, Y. S. Bioinspired Exosome-Mimetic Nanovesicles for Targeted Delivery of Chemotherapeutics to Malignant Tumors. *ACS Nano* **2013**, *7*, 7698−7710.

(10) Kamerkar, S.; LeBleu, V. S.; Sugimoto, H.; Yang, S.; Ruivo, C. F.; Melo, S. A.; Lee, J. J.; Kalluri, R. Exosomes facilitate therapeutic targeting of oncogenic KRAS in pancreatic cancer. *Nature* **2017**, *546*, 498−503.

(11) Xu, Z.; Zeng, S.; Gong, Z.; Yan, Y. Exosome-based immunotherapy: a promising approach for cancer treatment. *Mol. Cancer* **2020**, *19*, 160.

(12) Choo, Y. W.; Kang, M.; Kim, H. Y.; Han, J.; Kang, S.; Lee, J.-R.; Jeong, G.-J.; Kwon, S. P.; Song, S. Y.; Go, S.; Jung, M.; Hong, J.; Kim, B.-S. M1 Macrophage-Derived Nanovesicles Potentiate the Anticancer Efficacy of Immune Checkpoint Inhibitors. *ACS Nano* **2018**, *12*, 8977−8993.

(13) Chen, Y.; Song, Y.; Du, W.; Gong, L.; Chang, H.; Zou, Z. Tumor-associated macrophages: an accomplice in solid tumor progression. *J. Biomed. Sci.* **2019**, *26*, 78.

(14) Zhang, F.; Parayath, N. N.; Ene, C. I.; Stephan, S. B.; Koehne, A. L.; Coon, M. E.; Holland, E. C.; Stephan, M. T. Genetic

programming of macrophages to perform anti-tumor functions using targeted mRNA nanocarriers. *Nat. Commun.* **2019**, *10*, 3974.
(15) Wang, Y.; Zhao, M.; Liu, S.; Guo, J.; Lu, Y.; Cheng, J.; Liu, J. Macrophage-derived extracellular vesicles: diverse mediators of pathology and therapeutics in multiple diseases. *Cell Death Dis.* **2020**, *11*, 924.
(16) Hwang, D. W.; Choi, H.; Jang, S. C.; Yoo, M. Y.; Park, J. Y.; Choi, N. E.; Oh, H. J.; Ha, S.; Lee, Y.-S.; Jeong, J. M.; Gho, Y. S.; Lee, D. S. Noninvasive imaging of radiolabeled exosome-mimetic nanovesicle using 99mTc-HMPAO. *Sci. Rep.* **2015**, *5*, 15636.
(17) Pozzi, D.; Colapicchioni, V.; Caracciolo, G.; Piovesana, S.; Capriotti, A. L.; Palchetti, S.; De Grossi, S.; Riccioli, A.; Amenitsch, H.; Laganà, A. Effect of polyethyleneglycol (PEG) chain length on the bio−nano-interactions between PEGylated lipid nanoparticles and biological fluids: from nanostructure to uptake in cancer cells. *Nanoscale* **2014**, *6*, 2782−2792.
(18) Saw, P. E.; Park, J.; Lee, E.; Ahn, S.; Lee, J.; Kim, H.; Kim, J.; Choi, M.; Farokhzad, O. C.; Jon, S. Effect of PEG pairing on the efficiency of cancer-targeting liposomes. *Theranostics* **2015**, *5*, 746−754.
(19) Lee, W.; Jeon, M.; Choi, J.; Oh, C.; Kim, G.; Jung, S.; Kim, C.; Ye, S.-J.; Im, H.-J. Europium-Diethylenetriaminepentaacetic Acid Loaded Radioluminescence Liposome Nanoplatform for Effective Radioisotope-Mediated Photodynamic Therapy. *ACS Nano* **2020**, *14*, 13004−13015.
(20) Jeon, M.; Kim, G.; Lee, W.; Baek, S.; Jung, H. N.; Im, H.-J. Development of theranostic dual-layered Au-liposome for effective tumor targeting and photothermal therapy. *J. Nanobiotechnol.* **2021**, *19*, 262.
(21) Najlah, M.; Said Suliman, A.; Tolaymat, I.; Kurusamy, S.; Kannappan, V.; Elhissi, A. M. A.; Wang, W. Development of Injectable PEGylated Liposome Encapsulating Disulfiram for Colorectal Cancer Treatment. *Pharmaceutics* **2019**, *11*, 610.
(22) Ren, H.; He, Y.; Liang, J.; Cheng, Z.; Zhang, M.; Zhu, Y.; Hong, C.; Qin, J.; Xu, X.; Wang, J. Role of Liposome Size, Surface Charge, and PEGylation on Rheumatoid Arthritis Targeting Therapy. *ACS Appl. Mater. Interfaces* **2019**, *11*, 20304−20315.
(23) Di, J.; Gao, X.; Du, Y.; Zhang, H.; Gao, J.; Zheng, A. Size, shape, charge and "stealthy" surface: Carrier properties affect the drug circulation time in vivo. *Asian J. Pharm. Sci.* **2021**, *16*, 444−458.
(24) Smyth, T.; Kullberg, M.; Malik, N.; Smith-Jones, P.; Graner, M. W.; Anchordoquy, T. J. Biodistribution and delivery efficiency of unmodified tumor-derived exosomes. *J. Controlled Release* **2015**, *199*, 145−155.
(25) Jin, S.; Ye, K. Nanoparticle-Mediated Drug Delivery and Gene Therapy. *Biotechnol. Prog.* **2007**, *23*, 32−41.
(26) Kabanov, A. V.; Gendelman, H. E. Nanomedicine in the diagnosis and therapy of neurodegenerative disorders. *Prog. Polym. Sci.* **2007**, *32*, 1054−1082.
(27) Shi, S.; Li, T.; Wen, X.; Wu, S. Y.; Xiong, C.; Zhao, J.; Lincha, V. R.; Chow, D. S.; Liu, Y.; Sood, A. K.; Li, C. Copper-64 Labeled PEGylated Exosomes for In Vivo Positron Emission Tomography and Enhanced Tumor Retention. *Bioconjugate Chem.* **2019**, *30*, 2675−2683.
(28) Kooijmans, S. A. A.; Fliervoet, L. A. L.; van der Meel, R.; Fens, M. H. A. M.; Heijnen, H. F. G.; van Bergen en Henegouwen, P. M. P.; Vader, P.; Schiffelers, R. M. PEGylated and targeted extracellular vesicles display enhanced cell specificity and circulation time. *J. Controlled Release* **2016**, *224*, 77−85.
(29) Emam, S. E.; Elsadek, N. E.; Abu Lila, A. S.; Takata, H.; Kawaguchi, Y.; Shimizu, T.; Ando, H.; Ishima, Y.; Ishida, T. Anti-PEG IgM production and accelerated blood clearance phenomenon after the administration of PEGylated exosomes in mice. *J. Controlled Release* **2021**, *334*, 327−334.
(30) Orecchioni, M.; Ghosheh, Y.; Pramod, A. B.; Ley, K. Macrophage Polarization: Different Gene Signatures in M1(LPS+) vs. Classically and M2(LPS-) vs. Alternatively Activated Macrophages. *Front. Immunol.* **2019**, *10*, 1084.
(31) Lee, C.; Jeong, H.; Bae, Y.; Shin, K.; Kang, S.; Kim, H.; Oh, J.; Bae, H. Targeting of M2-like tumor-associated macrophages with a melittin-based pro-apoptotic peptide. *J. Immunother. Cancer* **2019**, *7*, 147.

Recommended by ACS

Bacterial Outer Membrane Vesicles Presenting Programmed Death 1 for Improved Cancer Immunotherapy via Immune Activation and Checkp...

Yao Li, Guangjun Nie, *et al.*
NOVEMBER 24, 2020
ACS NANO
READ

Hybrid Vesicles Based on Autologous Tumor Cell Membrane and Bacterial Outer Membrane To Enhance Innate Immune Response and Personalized Tumor...

Mei-Zhen Zou, Xian-Zheng Zhang, *et al.*
OCTOBER 18, 2021
NANO LETTERS
READ

Antigen Delivery to Antigen-Presenting Cells for Adaptive Immune Response by Self-Assembled Anionic Polysaccharide Nanogel Vaccines

Risako Miura, Kazunari Akiyoshi, *et al.*
DECEMBER 04, 2019
BIOMACROMOLECULES
READ

Importance of the Phospholipid Core for Mucin Hydrogel Penetration and Mucosal Cell Uptake of Maltodextrin Nanoparticles

François Fasquelle, Didier Betbeder, *et al.*
AUGUST 03, 2020
ACS APPLIED BIO MATERIALS
READ

Get More Suggestions >

https://doi.org/10.1021/acsabm.2c00246
ACS Appl. Bio Mater. 2022, 5, 2862−2869